New Technology for High-Speed and High-Resolution Optical Coherence Tomography[a]

J. G. FUJIMOTO,[b,c] B. BOUMA,[c] G. J. TEARNEY,[c]
S. A. BOPPART,[c] C. PITRIS,[c] J. F. SOUTHERN,[d]
AND M. E. BREZINSKI[d]

[c]*Department of Electrical Engineering and Computer Science*
and Research Laboratory of Electronics
Massachusetts Institute of Technology
Building 36-345
77 Massachusetts Avenue
Cambridge, Massachusetts 02139
and
[d]*Cardiac Unit*
Massachusetts General Hospital
Harvard Medical School
Boston, Massachusetts 02114

Optical coherence tomography (OCT) is an attractive technique for optical biopsy because it can permit the imaging of tissue microstructure *in situ* yielding micron-scale image resolution without the need for excision of a specimen and tissue processing. OCT is analogous to ultrasound B mode imaging except that it uses light rather than sound and performs imaging by measuring the backscattered intensity of light from structures in tissue.[1] The principles of OCT imaging are shown schematically in FIGURE 1. The OCT image is a gray scale or false color two-dimensional representation of backscattered light intensity in a cross-sectional plane. In medical imaging, the OCT image represents the differential backscattering contrast between different tissue types on a micron scale. In comparison to ultrasound, because OCT performs imaging using light, it can have one order of magnitude or more higher spatial resolution and can perform measurements noncontact.

OCT was originally developed and demonstrated in ophthalmology for performing high-resolution tomographic imaging of the retina and anterior eye.[2-4] Because the eye is transparent and provides easy optical access, it is well suited for diagnostic OCT imaging. OCT is especially promising for the diagnosis and management of retinal diseases because it can provide images of retinal pathology with 10-micron resolution, almost one order of magnitude higher than previously possible. To date, several thousand patients have been examined and horizontal

[a] This reserch is supported in part by the National Institutes of Health, Contract NIH-9-RO1-EY11289-10 (JGF), the Medical Free Electron Laser Program, Office of Naval Research, Contract N00014-94-1-0717 (JGF), the Air Force Office of Scientific Research, Contract F49620-95-1-0221 (JGF), the Joint Services Electronics Program, Contract DAAH04-95-1-0038 (JGF), the Whittaker Foundation, Contract 96-0205 (MEB), and the National Institutes of Health, Contract NIH-1-R29-HL55686-01A1 (MEB).

[b] Corresponding author.

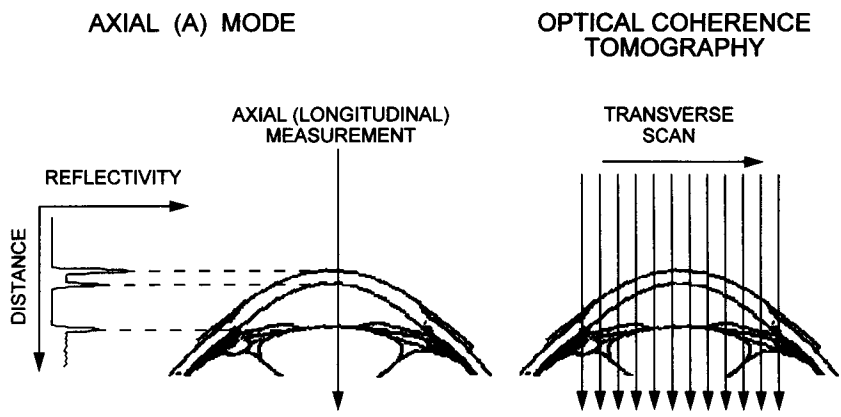

FIGURE 1. Schematic diagram showing how OCT imaging is performed. An optical beam is directed at the object to be imaged and backscattered light is measured as the beam is scanned across the object.

studies have been performed to assess the application of OCT for a number of macular diseases.[3,4] OCT is especially promising for the diagnosis and monitoring of diseases such as glaucoma and macular edema associated with diabetic retinopathy. In these contexts OCT permits the quantitative measurement of changes in retinal morphology such as the thickness of the retina or density of the retinal nerve fiber layer, which are associated with disease onset and progression. Because these changes often occur before the onset of physical symptoms, OCT can provide a powerful approach for the diagnosis and management of these diseases.

More recently OCT imaging has been demonstrated for imaging a wide range of nontransparent tissues.[5–9] In turbid media, imaging depth is limited by optical attenuation due to scattering and absorption. However, in most tissues imaging depths of 2–3 mm can be achieved using a dynamic range of 100 dB. OCT has been applied *in vitro* to image arterial pathology where it can differentiate plaque morphology with superior resolution to ultrasound.[10,11] Imaging studies have also been performed to investigate applications in gastroenterology, urology, and neurosurgery.[12–14] OCT has also been applied *in vivo* to image developing biological specimens (African frog, leopard frog, and zebrafish tadpoles and embryos). In this context OCT can permit the repeated imaging of developing morphology without the need to sacrifice specimens.[15–17]

OCT is based on optical ranging and the high-resolution, high-dynamic range detection of backscattered light as a function of optical delay. In contrast to ultrasound, because the velocity of light is extremely high, the echo time delay of reflected light cannot be measured directly. Interferometric detection techniques must therefore be used. One of the most attractive methods for performing this measurement is to use low-coherence interferometry or optical coherence domain reflectometry. (FIG. 2) Low-coherence interferometry was first developed for measuring reflections in fiber optics and optoelectronic devices and was first demonstrated in ophthalmology for measurements of axial eye length and corneal thickness.[18–21]

Coherence domain ranging uses heterodyne detection of light backscattered from the sample. Interference of the light reflected from the sample arm and

reference arm of a Michelson interferometer (FIG. 2) can occur only when the optical path lengths of the two arms match to within the coherence length of the optical source. As the reference arm optical path length is scanned, backscattering sites within the sample are localized. Interferograms detected at the output port of the interferometer are bandpass filtered, demodulated, digitized and stored on a computer. OCT tomographic images are composed of sequentially recorded axial scans as either the sample is scanned transverse to the incident beam, or the probing beam itself is scanned.

The transverse resolution achieved with an OCT imaging system is determined by the focused spot size in analogy with conventional microscopy. The transverse resolution is given by:

$$\Delta x = (4\lambda/\pi)(f/d)$$

Where d is the spot size on the objective lens and f is its focal length. High transverse resolution can be obtained by using a large numerical aperture and focusing the beam to a small spot size. In addition, the transverse resolution is also related to the depth of focus or the confocal parameter $2z_R$ (two times the Raleigh range):

$$2z_R = \pi\Delta x^2/2\lambda$$

Thus, increasing the transverse resolution trades off against a reduced depth of field. Typically, the confocal parameter or depth of focus is chosen to match the

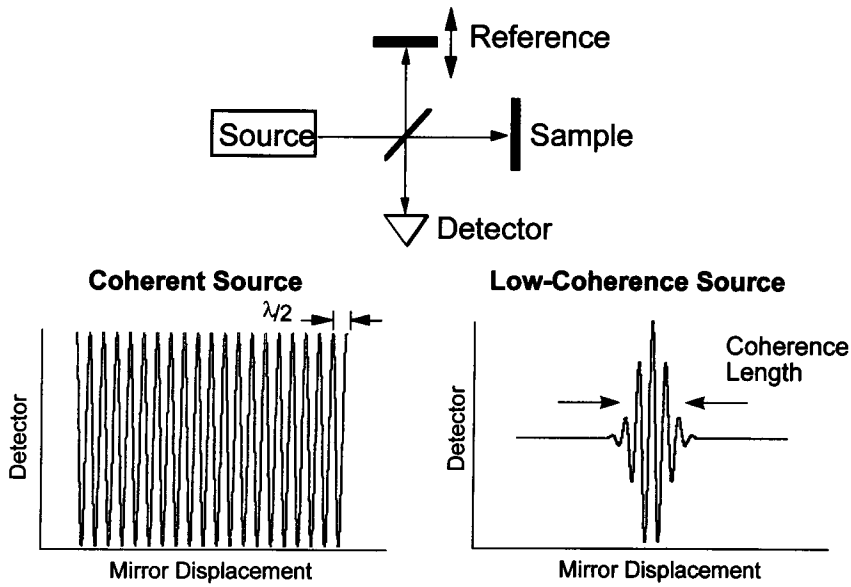

FIGURE 2. Schematic showing the basic concept of low-coherence interferometry. Using a short coherence length light source and a Michelson type interferometer, interference fringes are observed only when the path lengths of the two interferometer arms are matched to within a coherence length.

desired depth of imaging. Increased resolution may also be obtained by spatially tracking the focus.

Unlike conventional microscopy, the axial resolution in OCT images is determined by the coherence length of the light source. If a single reflection is measured to define the point spread function of the OCT measurement, the signal detected at the output port of the interferometer is the electric-field autocorrelation of the source. The coherence length is the spatial width of the field autocorrelation. The envelope of the field autocorrelation is equivalent to the Fourier transform of its power spectrum. Thus the width of the autocorrelation function, or the axial resolution, is inversely proportional to the width of the power spectrum. For a source with a Gaussian spectral distribution, the axial resolution Δz is given:

$$\Delta z = \frac{2\mathrm{Ln}2}{\pi}\frac{\lambda^2}{\Delta\lambda},$$

where Δz and $\Delta\lambda$ are the full-widths at half-maximum (FWHM) of the autocorrelation function and power spectrum, respectively, and λ is the source central wavelength. Thus, broad bandwidth optical sources are required to achieve high axial resolution.

Finally, the signal-to-noise ratio (SNR) of detection is given by the optical power backscattered from the sample divided by the noise equivalent bandwidth (NEB):

$$SNR = 10\,Log\left(\frac{\eta}{\hbar\omega}\frac{P_{SAM}}{NEB}\right),$$

The majority of OCT imaging systems to date have used superluminescent diodes (SLDs) as low-coherence light sources. SLDs are attractive because they are compact, high efficiency, and low noise. However, output powers are typically limited to several hundred microwatts and available bandwidths permit imaging with 10–15-micron resolution. Other superluminescent sources such as fluorescence from organic dyes and from $Ti:Al_2O_3$ have been demonstrated to achieve resolution as low as 2 μm.[22,23] However, these superfluorescent sources have limited output powers, and in order to achieve high-speed imaging with high SNR, tens of milliwatts are typically required.

Recent advances in short-pulse, solid-state laser technology make it attractive for OCT imaging. Femtosecond solid-state lasers can generate tunable low-coherence light at power levels well in excess of 100 mW. Kerr lens modelocking (KLM) has been demonstrated as a technique for generating tunable ultrashort pulses in a variety of solid state lasers. Pulses with durations below 10 fs have been achieved in $Ti:Al_2O_3$ and pulse durations of <100 fs have been achieved in several near-infrared laser materials such as $Cr^{4+}:Mg_2SiO_4$ and $Cr^{4+}:YAG$.[24-26] These three materials cover a range of wavelengths in the near infrared. Modelocked operation has been demonstrated across the full tuning range in $Ti:Al_2O_3$ from 0.7 μm to 1.1 μm, while in $Cr^{4+}:Mg_2SiO_4$ and $Cr^{4+}:YAG$, short-pulse generation at selected wavelength ranges has been achieved, with the ultimate potential of tuning from 1.18 μm to 1.36 μm and from 1.35 μm to 1.64 μm, respectively.

FIGURE 3 shows an example of a 10-fs pulse generated from a $Ti:Al_2O_3$ and the corresponding spectrum. The figure shows an example of a collinear intensity correlation and emphasizes the fact that pulse durations of 10 fs consist of only a few cycles of light. The $Ti:Al_2O_3$ laser source is pumped by an argon laser and generates average powers of up to 400 mW, although powers of several tens of mW are sufficient for OCT imaging.

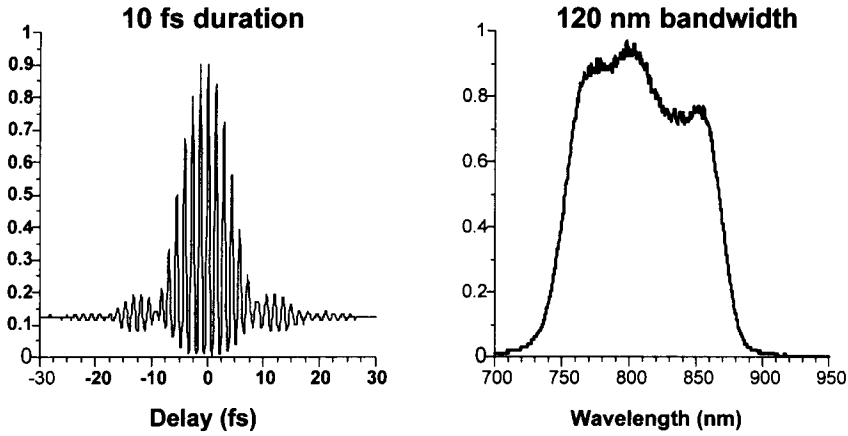

FIGURE 3. Intensity autocorrelation and spectrum of 10-fs pulses generated by Ti:Al_2O_3 laser.

The OCT system is implemented using a fiber optic coupler for the Michelson interferometer (FIG. 4). One of the arms of the interferometer is used to deliver and scan the optical beam on the sample, while the other, functioning as a reference arm, has a high-speed scanning delay. The delay can be implemented using a number of techniques including a high-speed scanning retroreflector as well as PZT actuators. The interference from the sample and the reference is detected and demodulated. In some cases a dual-detector geometry is used where the output of

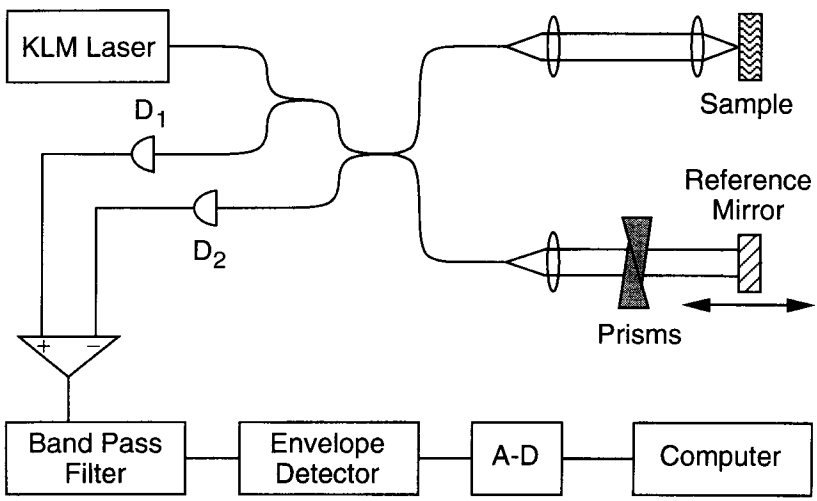

FIGURE 4. Schematic representation of OCT system implemented using fiber optics.

two detectors that detect the optical interference in quadrature was subtracted. This results in an addition of the interference signal while canceling the background signal from the reference beam and reducing excess noise. A pair of prisms, which functions as a variable thickness of glass, is used to balance dispersion in the two arms of the interferometer.

For OCT imaging an approximately 100-mW laser output is coupled into the single-mode fiber of the interferometer. Normal material dispersion in the fiber produces a significant pulse broadening for pulses of these short durations and large bandwidths. It is important to note, however, that the axial resolution in OCT depends on the Fourier transform of the spectrum and not on the pulse duration. This spectrum is unchanged in linear propagation, and hence the axial resolution is not degraded. it is important however, that dispersion be precisely balanced in the two arms of the interferometer.

The large bandwidths available from short-pulse, solid-state lasers yield a significant increase in resolution compared to superluminescent diode sources. FIGURE 5 show a comparison of an OCT image of an onion performed with a standard resolution SLD source and the KLM $Ti:Al_2O_3$ system.[27] In both images the trans-

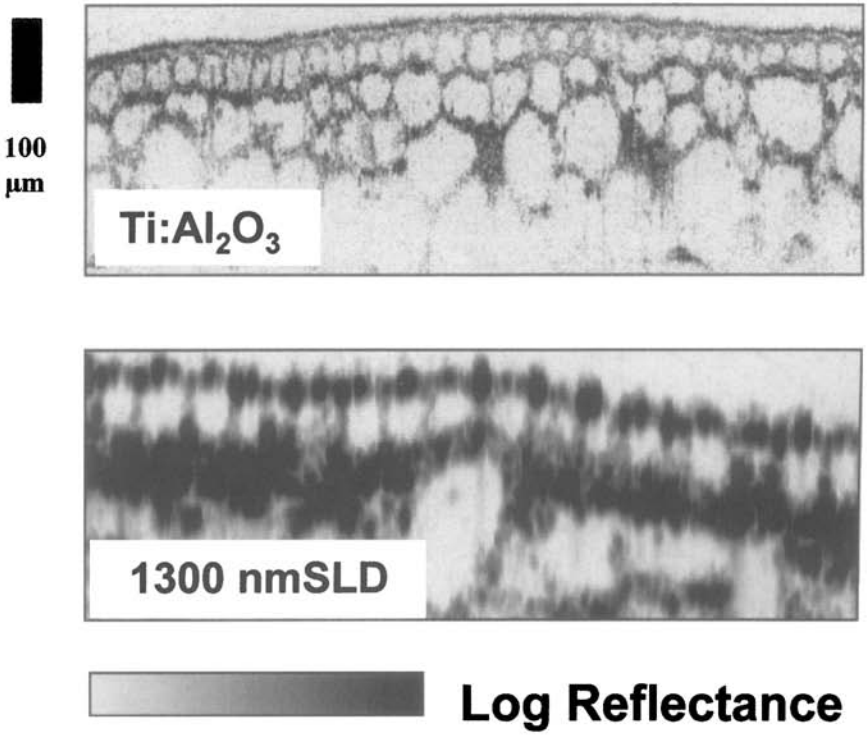

FIGURE 5. Image of an onion acquired with the $Ti:Al_2O_3$ source OCT system. The high resolution (4 μm) allows the cellular structure to be visualized. The image measures 1 mm in depth by 3 mm transverse. Comparison with standard 15-μm resolution obtained by an SLD is shown.

verse resolution determined by the focusing objectives is approximately matched to the longitudinal resolution as determined by the system bandwidth. In the high-resolution image the optical beam diameter is 5 mm in the focal plane, which is centered on the first horizontal cell layer. The corresponding confocal parameters is 40 μm, the approximate dimension of the cells in this layer. At greater depths, resolution degradation due to divergence becomes apparent. Translating the focal plane allows high-resolution imaging to a depth of ~600 μm in an onion, where multiple scattering becomes significant. The confocal parameter in an SLD lower-resolution image is 350 μm. Both of these images were acquired in 2.5 seconds by sampling 120 vertical and 360 horizontal pixels.

Although the $Ti:Al_2O_3$ laser source can produce very high-resolution OCT imaging, the 800-nm wavelength is not optimum for imaging in scattering tissues. The depth to which OCT imaging is possible is limited by the penetration depth of the incident beam. Scattering and absorption of the tissue produce attenuation of the backscattered signal, which determines the imaging depth. Studies of the optical properties of tissue show that scattering diminishes rapidly with increasing wavelength throughout the visible and infrared spectral regions. Absorption in tissue is dominated by absorption features from melanin, hemoglobin, and water. For light near 800 nm wavelength, absorption is relatively weak and scattering is the dominant mechanism of attenuation. At longer wavelengths, such as 2.0 μm, scattering is minimal but water absorption dominates. At a wavelength of 1.3 μm, water absorption is still minimal but scattering is significantly decreased in comparison to 800 nm. For this reason the $Cr^{4+}:Mg_2SiO_4$ laser, which operates in 1.3 μm spectral range, is best suited for OCT imaging in biological tissues.

$Cr^{4+}:Mg_2SiO_4$ is a new broadband tunable solid-state laser material, which is pumpable at 1 μm and operates in the 1.18–1.36-μm wavelength range.[25] Pulse durations as short as 25 fs have been produced by applying Kerr lens modelocking to a Nd:YAG-pumped $Cr^{4+}:Mg_2SiO_4$ oscillator. The laser used in this study consists of 1.0 cm $Cr^{4+}:Mg_2SiO_4$ crystal with an absorption coefficient of 1.8 cm^{-1} in a standard z-cavity configuration with a 6% output coupler. Dispersion compensation is provided by a pair of SF6 prisms. The laser is pumped with 6.0 W at 1.06 μm from a diode pumped Nd:YAG laser and generates 300 mW of modelocked output power. The spectrum of the laser pulses has a FWHM bandwidth of 50 nm, which corresponds to a coherence length of 15 μm. Because this laser is pumped by a diode-pumped Nd:YAG, it had significantly lower excess noise compared to the argon-pumped $Ti:Al_2O_3$ laser.

The $Cr^{4+}:Mg_2SiO_4$ laser source permits the rapid acquisition of 15-μm-resolution OCT images with signal-to-noise levels exceeding 115 dB. However, for many imaging applications, it is desirable to achieve higher resolutions. In order to increase the resolution the spectrum of these laser pulses can be broadened by using nonlinear self-phase modulation.[28] In order to generate a good quality spectral shape, self-phase modulation must be performed using dispersion-shifted fiber, so that the zero of dispersion does not occur at a wavelength within the bandwidth to be generated. Spectral broadening is produced by coupling 100 mW of average power in a Corning SMF/DS™ CPC3 dispersion-shifted fiber (zero group velocity dispersion at 1.55 μm) and reduces the FWHM of the coherence length to 5.7 μm.

The high resolution combined with the increased penetration associated with 1.3 μm wavelengths is ideal for OCT imaging in a wide range of application. FIGURE 6 shows an *in vivo* OCT image of gill structure in a developing tadpole (*Xenopus laevis*) generated using the high-resolution $Cr^{4+}:Mg_2SiO_4$ OCT system. The transverse resolution, determined by the focused beam spot size, was adjusted to approximately match the axial resolution of the self-phase modulated laser source,

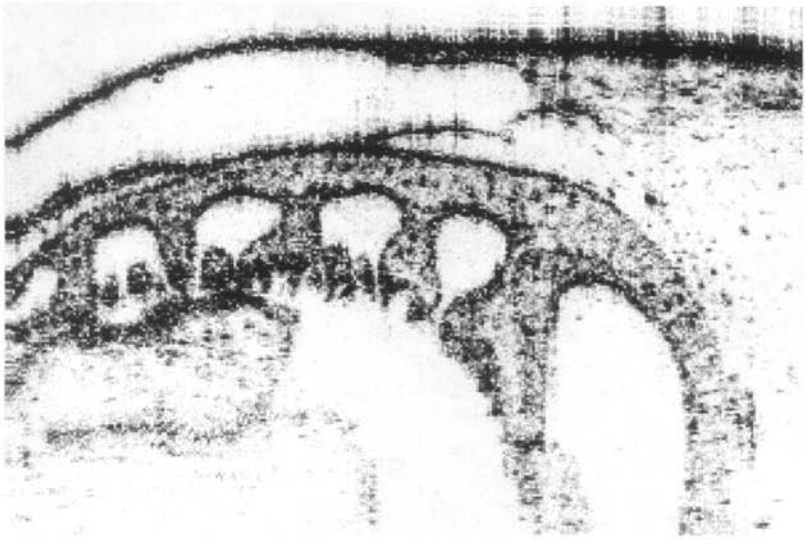

FIGURE 6. OCT image of the gill structure in a developing tadpole (*Xenopus laevis*) measured using a high-resolution $Cr^{4+}:Mg_2SiO_4$ laser source. The axial resolution is 5 μm and the image spans an area 1 mm $\times$ 1.5 mm.

5 μm. Using 2 mW of incident optical power, the measured signal-to-noise is 115 dB. The image is composed of 600 axial scans at transverse positions 3 μm apart. Each axial scan covers a depth of 0.5 mm and contains 200 pixels. The total image was acquired in 30 seconds. The high resolution of this system permits the visualization of tissue microstructure including cell membranes and intercellular spaces.

Solid-state laser sources are attractive not only because they enable OCT imaging at unprecedented high-resolution, but also because the high output powers enable rapid image acquisition.[29] Performing OCT imaging within living specimens requires that the imaging be performed rapidly compared to any motion in order to avoid blurring artifacts. In addition, the clinical application of OCT will require real-time visualization for guidance. FIGURE 7 shows an example of high-speed imaging of cardiac function in an *in vivo* tadpole (*Xenopus laevis*). The image consists of 300 $\times$ 250 pixels corresponding to 3.0 mm $\times$ 2.2 mm and were acquired at a rate of four images per second. The axial resolution in these images was 15 μm.

Finally, in order to perform OCT imaging in future clinical applications, it is necessary to develop OCT catheter/endoscopes. This OCT technology enables imaging of internal organ systems such as the cardiovascular system, the gastrointestinal tract, and the urinary tract. Since OCT is fiber-optically based, it can be integrated into a wide range of catheter/endoscope designs. FIGURE 8 shows a schematic diagram of a transverse scanning OCT catheter. The catheter consists of a single-mode optical fiber in a speedometer cable structure with focusing optics for the output beam at the distal end. The optical elements are encased in a transparent housing. The catheter performs transverse imaging by scanning a radically directed OCT beam in a circumferential pattern to construct a transluminal image.[30] FIGURE 9 shows imaging of an intact, *in vitro* saphenous vein comparing the OCT catheter/endoscope to a 30-MHz intravascular ultrasound (IVUS) image.

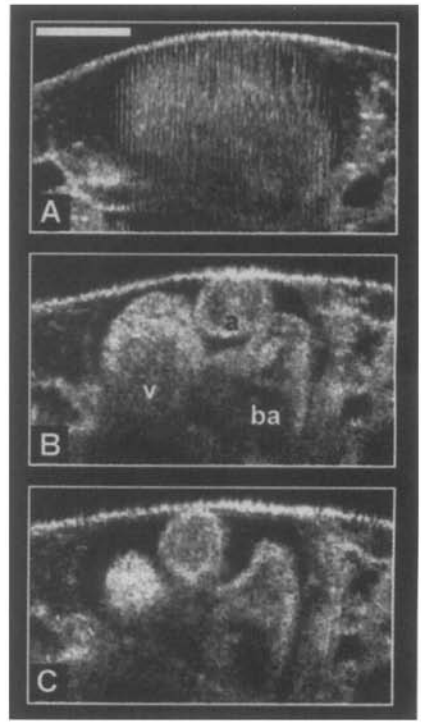

FIGURE 7. OCT image of an *in vivo* *Xenopus laevis* (African frog) heart acquired using the high-speed OCT system in 0.25 seconds and standard low speed system (30 sec per image). The anatomy of the beating heart can be clearly visualized, including the pericardium (pc), the atrium (a), the ventricle (v), and the bulbus arteriosus (ba). The *bar* represents 500 μm.

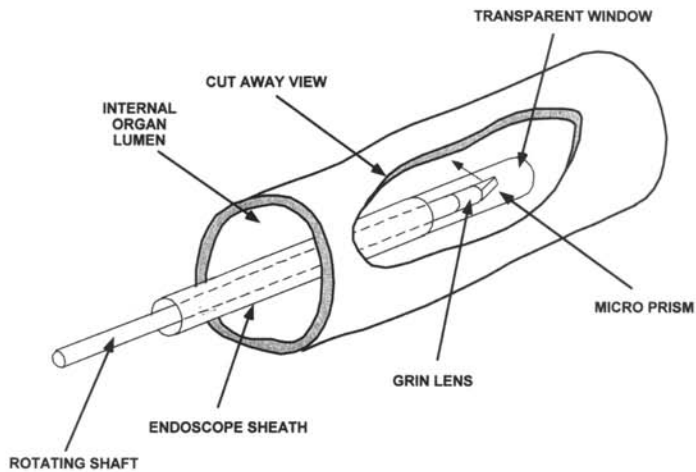

FIGURE 8. Schematic of OCT catheter-endoscope for transverse imaging.

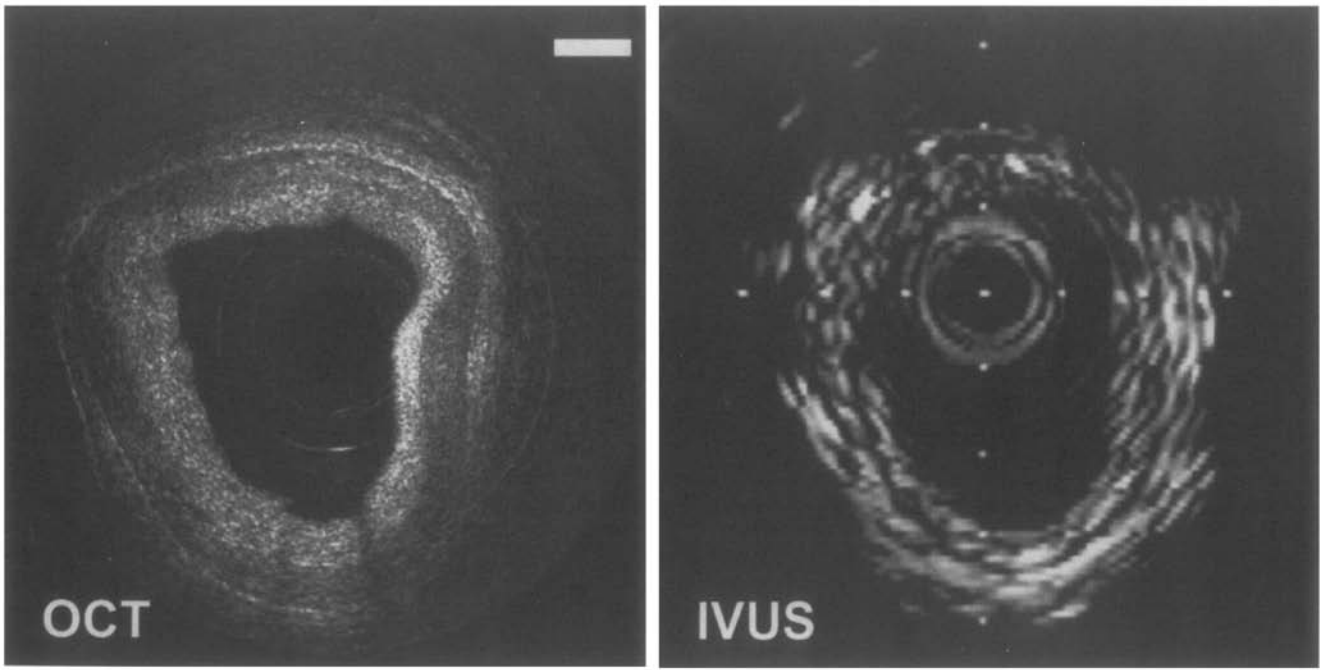

FIGURE 9. Comparison images of *in vitro* human saphenous vein using the OCT catheter-endoscope (*left*) and a standard 30 MHz intravascular ultrasound (IVUS) catheter (*right*) during coronary artery intimal hyperplasia.

The OCT image shows a significant enhancement in resolution and the capability to differentiate tissue morphology. In recent studies we have extended these results to perform the first *in vivo* catheter/endoscopic imaging in an animal model.[31]

The development of high-resolution and high-speed OCT technology as well as OCT-compatible catheter-endoscopes represents essential steps towards enabling OCT imaging for *in vivo* endoscopic optical biopsy of biological tissues. OCT can perform micron-scale, real-time imaging of cellular and architectural morphology *in situ* without the need for excision and histological processing and thus is a powerful technique for optical biopsy. The capability to perform rapid *in situ* imaging can be used in a variety of clinical scenarios including: 1. To guide conventional biopsy and improve false negative rates due to sampling errors, 2. To perform imaging of tissue microstructure in which conventional biopsy would be hazardous, and 3. To guide microsurgical intervention. Thus OCT imaging has the potential to have a significant impact on the diagnosis and clinical management of many diseases.

SUMMARY

Optical coherence tomography (OCT) is an optical imaging technique that is capable of performing micron-scale, cross-sectional imaging of internal microstructure in biological systems. OCT is analogous to ultrasound B mode imaging except that it uses light rather than sound and performs imaging by measuring the backscattered intensity of light from structures in tissue. We describe recent advances in OCT technology including the application of short pulse solid state lasers based on $Ti:Al_2O_3$ and $Cr:Mg_2SiO_4$ to enable high-resolution, high-speed imaging as well as the development of OCT catheter/endoscope delivery to permit imaging of internal organ systems. OCT enables the nonexcisional, *in situ*, real-time imaging of tissue microstructure and is thus a powerful and promising technique for optical biopsy.

REFERENCES

1. Huang, D., E. A. Swanson, C. P. Lin, J. S. Schuman, W. G. Stinson, W. Chang, M. R. Hee, T. Flotte, K. Gregory, C. A. Puliafito & J. G. Fujimoto. 1991. Optical coherence tomography. Science **254:** 1178–1181.
2. Hee, M. R., J. A. Izatt, E. A. Swanson, D. Huang, C. P. Lin, J. S. Schuman, C. A. Puliafito & J. G. Fujimoto. 1995. Optical coherence tomography of the human retina. Arch. Ophthalmol. **113:** 325–332.
3. Puliafito, C. A., M. R. Hee, C. P. Lin, E. Reichel, J. S. Schuman, J. S. Duker, J. A. Izatt, E. A. Swanson & J. G. Fujimoto. 1995. Imaging of macular disease with optical coherence tomography (OCT). Ophthalmology **102:** 217–229.
4. Puliafito, C. A., M. R. Hee, J. S. Schuman & J. G. Fujimoto. 1995. Optical Coherence Tomography of Ocular Diseases. Slack, Inc. Thorofare, NJ.
5. Schmitt, J. M., A. Knuttel & R. F. Bonner. 1993. Measurement of the optical properties of biological tissue using low-coherence reflectometry. Appl. Opt. **32:** 6032.
6. Fujimoto, J. G., M. E. Brezinski, G. J. Tearney, S. A. Boppart, B. E. Bouma, M. R. Hee, J. F. Southern & E. A. Swanson. 1995. Biomedical imaging and optical biopsy using optical coherence tomography. Nat. Med. **1:** 970–972.
7. Schmitt, J. M., M. J. Yadlowsky & R. F. Bonner. 1995. Subsurface imaging of living skin with optical coherence microscopy. Dermatology **191:** 93–98.
8. Sergeev, A., B. Gelikonov, G. Gelikonov, F. Feldchtein, K. Pravdenki, R. Kuranov, N. Gladkova, V. Pochinko, G. Petrova & N. Nikulin. 1995. High-spatial-resolution optical-coherence tomography of human skin and mucous membranes. *In*

OSA Technical Digest Series. Vol. 15: paper CThN4. Optical Society of America. Washington, DC.

9. SCHMITT, J. M., A. KNUTTEL, M. YADLOWSKY & A. A. ECKHAUS. 1994. Optical coherence tomography of a dense tissue: statistics of attenuation and backscattering. Phys. Med. Biol. **39:** 1705.
10. BREZINSKI, M. E., G. J. TEARNEY, B. E. BOUMA, J. A. IZATT, M. R. HEE, E. A. SWANSON, J. F. SOUTHERN & J. G. FUJIMOTO. 1996. Optical coherence tomography for optical biopsy: properties and demonstration of vascular pathology. Circulation **93:** 1206–1213.
11. TEARNEY, G. J., M. E. BREZINSKI, S. A. BOPPART, B. E. BOUMA, N. WEISSMAN, J. F. SOUTHERN, E. A. SWANSON & J. G. FUJIMOTO. 1996. Catheter-based optical imaging of a human coronary artery. Circulation **94:** 3013.
12. TEARNEY, G. J., M. E. BREZINSKI, B. E. BOUMA, J. F. SOUTHERN, S. A. BOPPART & J. G. FUJIMOTO. 1997. Optical biopsy in human gastrointestinal tissues using optical coherence tomography. Am. J. Gastroenterol. In press.
13. TEARNEY, G. J., M. E. BREZINSKI, J. F. SOUTHERN, B. E. BOUMA, S. A. BOPPART & J. G. FUJIMOTO. 1997. Optical biopsy in human urologic tissue using optical coherence tomography. J. Urol. **157**. In press.
14. BREZINSKI, M. E., G. J. TEARNEY, S. A. BOPPART, E. A. SWANSON & J. G. FUJIMOTO. 1997. Optical biopsy with optical coherence tomography, feasibility for surgical diagnostics. J. Surg. Res. In press.
15. BOPPART, S. A., M. E. BREZINSKI, B. E. BOUMA, G. J. TEARNEY & J. G. FUMIMOTO. 1996. Investigation of developing embryonic morphology using optical coherence tomography. Dev. Biol. **177:** 54–63.
16. BOPPART, S. A., B. E. BOUMA, M. E. BREZINSKI, G. J. TEARNEY & J. G. FUJIMOTO. 1996. Imaging developing neural morphology using optical coherence tomography. J. Neurosci. Methods **70:** 65–72.
17. BOPPART, S. A., G. J. TEARNEY, B. E. BOUMA, J. F. SOUTHERN, M. E. BREZINSKI & J. G. FUJIMOTO. 1997. Noninvasive assessment of the developing *xenopus* cardiovascular system using optical coherence tomography. Proc. Natl. Acad. Sci. USA **94:** 4256–4261.
18. TAKADA, K., I. YOKOHAMA, K. CHIDA & J. NODA. 1987. New measurement system for fault location in optical waveguide devices based on an interferometric technique. Appl. Opt. **26:** 1603.
19. FERCHER, A. F., K. MENGEDOHT & W. WERNER. 1988. Eye-length measurement by interferometry with partially coherent light. Opt. Lett. **13:** 186.
20. HITZENBERGER, C. K. 1991. Measurement of the axial eye length by laser Doppler interferometry. Invest. Ophthalmol. Vis. Sci. **32:** 616.
21. IZATT, J. A., M. R. HEE, E. A. SWANSON, C. P. LIN, D. HUANG, J. S. SCHUMAN, C. A. PULIAFITO & J. G. FUJIMOTO. 1994. Micrometer-scale resolution imaging of the anterior eye *in vivo* with optical coherence tomography. Arch. Ophth. **112:** 1584–1589.
22. LIU, H.-H., P.-H. CHENG & J. WANG. 1993. Spatially coherent white-light interferometer based on a point fluorescent source. Opt. Lett. **18:** 678.
23. CLILVAZ, X., F. MARQUIS-WEIBLE & R.-P. SALATHE. 1994. 1.5 μm resolution optical low coherence reflectometry in biological tissues. Proc. Soc. Photo-Opt. Instrum. Eng. **2083:** 19.
24. SHOU, J. Z., G. TAFT, C. P. HUANG, M. M. MURNANE & H. C. KAPTEYN. 1994. Pulse evolution in a broad-bandwidth Ti:sapphire laser. Opt. Lett. **19:** 1149.
25. PETRICEVIC, V., S. K. GAYEN & R. R. ALFANO. 1988. Laser action in chromium activated forsterite for near infrared excitation: is $Cr4^+$ the lasing ion? Appl. Phys. Lett. **53:** 2590.
26. SEAS, A., V. PETRICEVIC & R. R. ALFANO. Generation of sub-100-fs pulses from a cw mode-locked chromium-doped forsterite laser. Opt. Lett. **17:** 937–939.
27. BOUMA, B. E., G. J. TEARNEY, S. A. BOPPART, M. R. HEE, M. E. BREZINSKI & J. G. FUJIMOTO. 1995. High-resolution optical coherence tomographic imaging using a mode-locked Ti: Al_2O_3 laser source. Opt. Lett. **20:** 1486–1488.
28. BOUMA, B. E., G. J. TEARNEY, I. P. BILINSKY, B. GOLUBOVIC & J. G. FUJIMOTO. 1996. Self-phase-modulated Kerr-lens mode-locked Cr:forsterite laser source for optical coherence tomography. Opt. Lett. **21:** 1839–1841.

29. TEARNEY, G. J., B. E. BOUMA, S. A. BOPPART, B. GOLUBOVIC, E. A. SWANSON & J. G. FUJIMOTO. 1996. Rapid acquisition of *in vivo* biological images using optical coherence tomography. Opt. Lett. **21:** 1408–1410.
30. TEARNEY, G. J., S. A. BOPPART, B. E. BOUMA, M. E. BREZINSKI, N. J. WEISSMAN, J. F. SOUTHERN & J. G. FUJIMOTO. 1996. Scanning single-mode fiber optic catheter-endoscope for optical coherence tomography. Opt. Lett. **21:** 1–3.
31. TEARNEY, G. J., M. E. BREZINSKI, B. E. BOUMA, S. A. BOPPART, C. PITRIS, J. F. SOUTHERN & J. G. FUJIMOTO. *In vivo* endoscopic optical biopsy with optical coherence tomography. Science. In press.